Fast and Accurate Retinal Identification System: Using Retinal Blood Vasculature Landmarks

Sidra Aleem, Bin Sheng, Ping Li, Po Yang, and David Dagan Feng, *Fellow, IEEE*

***Abstract*—The expansion of automation techniques and increased risk of identity theft have led emphasis on the tremendous need of automated identification system. Due to the high recognition accuracy and robustness to changes in human physiology, retinal biometric identification system has drawn much attention in this research field. In this paper, we aim to propose an automatic fast and accurate retinal identification system for the multisample dataset. The proposed approach uses a hybrid segmentation technique to segment out both thick/thin vessels for effectively balancing the difference of wavelet response between thick/thin blood vessels. As a result, recognition accuracy is improved. A Principle Component Analysis-based feature processing approach is proposed for efficiently reducing the dimensionality of a large number of vessels features. It significantly reduces computation time and accelerates the matching process in the retinal identification system. The proposed technique is validated on DRIVE, STARE, VARIA, RIDB, HRF, Messidor, DIARETDB0, and a large multisample per subject database created by authors using the images provided by Dr. Chen (Shanghai Jiao Tong University Affiliated Sixth People Hospital). Experimental results demonstrated that the proposed approach outperforms other existing techniques. Segmentation achieves an overall accuracy of 99.65% with the recognition rate of 99.40% on all these databases.**

***Index Terms*—Biometrics, PCA, retinal identification.**

Manuscript received October 9, 2018; accepted November 11, 2018. Date of publication November 15, 2018; date of current version July 3, 2019. This work was supported in part by the National Natural Science Foundation of China under Grant 61872241 and Grant 61572316, in part by the National Key Research and Development Program of China under Grant 2017YFE0104000 and Grant 2016YFC1300302, in part by the Macau Science and Technology Development Fund under Grant 0027/2018/A1, and in part by the Science and Technology Commission of Shanghai Municipality under Grant 18410750700, Grant 17411952600, and Grant 16DZ0501100. Paper no. TII-18-2653. *(Corresponding author: Bin Sheng.)*

S. Aleem and B. Sheng are with the Department of Computer Science and Engineering, Shanghai Jiao Tong University, Shanghai 200240, China (e-mail: sidraaleem1234@gmail.com; shengbin@sjtu.edu.cn).

P. Li is with the Faculty of Information Technology, Macau University of Science and Technology, Macau 999078, China (e-mail: pli@must.edu.mo).

P. Yang is with the Department of Computer Science, Liverpool John Moores University, Liverpool L3 3AF, U.K. (e-mail: P.Yang@ljmu.ac.uk).

D. D. Feng is with the Biomedical and Multimedia Information Technology Research Group, School of Information Technologies, The University of Sydney, Sydney, NSW 2006, Australia (e-mail: dagan.feng@sydney.edu.au).

Color versions of one or more of the figures in this paper are available online at http://ieeexplore.ieee.org.

Digital Object Identifier 10.1109/TII.2018.2881343

I. Introduction

THE expansion of automation technologies and increased risk of identity theft have led emphasis on the need of automated identification systems. Due to the claimed distinctiveness, biometric authentication approach is widely used for people identification based on their physical and behavioral traits [1]. Typical examples of biometric traits include face, fingerprint, ear, retina, iris, palm print, speech, signature, keystroke dynamics, gesture, and gait [2]–[7]. While some commonly commercial biometric identifiers like face or voice have provided a relatively medium level of security, they all suffer from various limitations: face recognition is widely affected by the changes in environment variations like light; voice can be easily recorded and used for the unauthorized network. Compared to these above biometric traits, the retina is an internal organ that lies at the back end of the eye which makes it resistant to forgery. Its morphological structure contains unique features as shown in Fig. 1. These features provide the basis for the distinction between different subjects [8], [9]. Therefore, the retinal image has advantages of the high uniqueness of vascular pattern across the human population, robustness to changes in human physiology, and hardly accessibility. These advantages, along with improvement in scanning technology, have contributed to the resurgence of interest in the retinal biometric in the last few years.

Typical automated retinal identification systems contain two important stages: utilization of advanced image segmentation approaches for reliable vasculature extraction, and selection and extraction of retinal features points from vasculature extraction for further algorithm training. The performance and outcome of two important stages directly decide recognition accuracy and efficiency of retinal identification systems. Thus, a variety of existing research work has been carried out to investigate novel algorithms in these two fields.

Regarding the vasculature extraction, early research on retina used matched filtering for blood vessel segmentation [10]. In [11], tracking method is proposed to obtain the vascular structure of the retina. Region-based threshold probing of the matched filter response [12], a combination of matched filters and likelihood ratio vesselness was proposed in [13] for segmentation. Morphological operations and a combination of nonlinear filtering and morphological operations were previously used to segment the vessels from the retinal image [14], [15]. However, automatic accurate segmentation of retinal vessels is a still very challenging task. The presence of noise, the low contrast

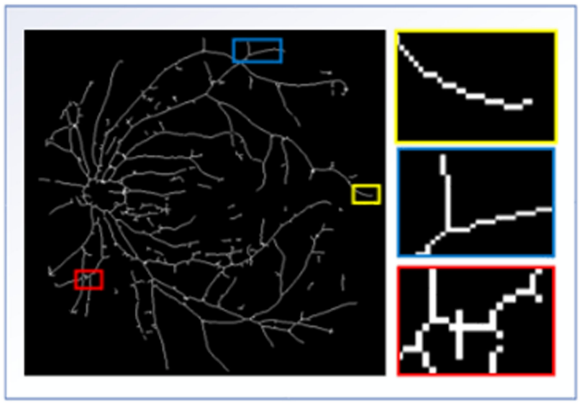

Fig. 1. Human Retinal Vasculature Network. End point, bifurcation, and crossing point are used as feature by the proposed system. Each of these feature points has been highlighted (Yellow = end point, Blue = bifurcation, Red = crossing over).

between vasculature and background, brightness, the variability of vessel width and shape are all obstacles further affecting the final recognition accuracy of the retinal identification system. As for the selection and extraction of retinal feature points, many works [4], [16]–[19] have used end points, bifurcations, crossing over, a combination of end points and bifurcation, a combination of bifurcations and crossing over, optic disc location as features. These features have demonstrated a great success in delivering high recognition accuracy, but this result requires complex and time-consuming operations to extract a large amount of feature points in each image among large sample databases. Also, the massive number and types of templates in different databases require much time to compare query images. Thus, how to accelerate the operations of feature processing for retinal identification systems is still a key problem.

In order to solve these problems, this paper attempts to improve the recognition accuracy and efficiency of retinal identification system. Accuracy is improved by using hybrid segmentation and efficiency is achieved by using principal component analysis (PCA) for template dimensionality reduction. Motivated by these above issues, this paper aims to propose an automatic fast and accurate retinal identification system for the multisample dataset. The idea is to use a hybrid segmentation technique to segment out both thick/thin vessels. Feature points are extracted to formulate the templates whose dimensionality is reduced by PCA. This step is crucial as it hastens the matching process. In the identification module, the query image template is generated. L2-norm is used to calculate the distance between the feature vector of the live template and the feature vector of all the templates stored in the database. Based on the distance total similarity measure TSM is calculated. The final decision is based on the TSM value. Fig. 2 gives an overview of the proposed system. The major contributions of this paper are as follows.

1) An automatic fast and accurate retinal identification system with hybrid segmentation for vasculature extraction is developed for the large-scale multisample retinal dataset. Our hybrid segmentation approach effectively balances the difference of wavelet response between thick/thin blood vessels. The use of a hybrid segmentation is more effective to retain as much retinal vasculature as possible and also prevents thin vessels from being discarded. As a result, recognition accuracy is improved.
2) PCA-based feature processing is proposed for efficiently reducing the dimensionality of a large number of vessels features toward multisample retinal dataset. The extracted features are projected into a subspace achieved by PCA. PCA approach ensures that principal components not only correspond to maximum variance, but also ensures that resulting set of features in the subspace are uncorrelated while retaining most of the information content. It could significantly reduce computation time and accelerate the matching process of retinal identification.
3) A comprehensive and in-depth experimental evaluation on practical large-scale multisample per subject dataset named biometric retinal identification database (BRDB) is designed for verifying the accuracy and efficiency of our method. The dataset consists of 1800 color retinal images of 200 subjects with nine samples per subject. The results show that our system could deliver a recognition accuracy up to 99.46% accuracy in industrial circumstance, which outweighs the state-of-the-art methods.

II. Related Work

EyeDentify company provided the first commercially available retinal identification system that uses a retina scanner called EyeDentification [20]. It maps vascular pattern on the retinal portion of the eyeball. Sadikoglu and Uzelaltinbulat [21] used the feature vector of the segmented image with a neural network. The neural network is trained by backpropagation. Fatima *et al.* [17] used a recursive supervised multilayered thresholding for accurate segmentation. Vascular ending and bifurcation are used as features. Mahalanobis distance is used as a similarity measure for identification. In [19], feature extraction is performed by using optic disc location as a reference point. Blood vessels that are around optic disc are used for feature generation. Köse *et al.* [22] proposed a retinal identification that employed a similarity measure and is capable of tolerating the transformations. In [23], Fourier transform coefficient and angular partitioning are used for feature detection. Euclidean distance is used in the matching process. Monisha and Seldevchristopher [24] used the crossing number technique to find features and voting for finding similarity. Sasidharan [25] used skeletonization for feature extraction. Similarity transformation is used for similarity check between reference and candidate image.

Akram *et al.* [16] formulated feature vector by calculating the distance and angle between feature points. Bifurcation is the chosen feature point. The accuracy was further improved by using both bifurcation and end points as features in [4]. Gabor filter is used for the extraction of feature points. The resulting feature vectors are stored in the database. The reference image and candidate images are matched using a SVM classifier [26]. In [18], branch points and crossing points are extracted from only those vessels that have a certain width. Geometric hashing is used to make features invariant. Crossing points and

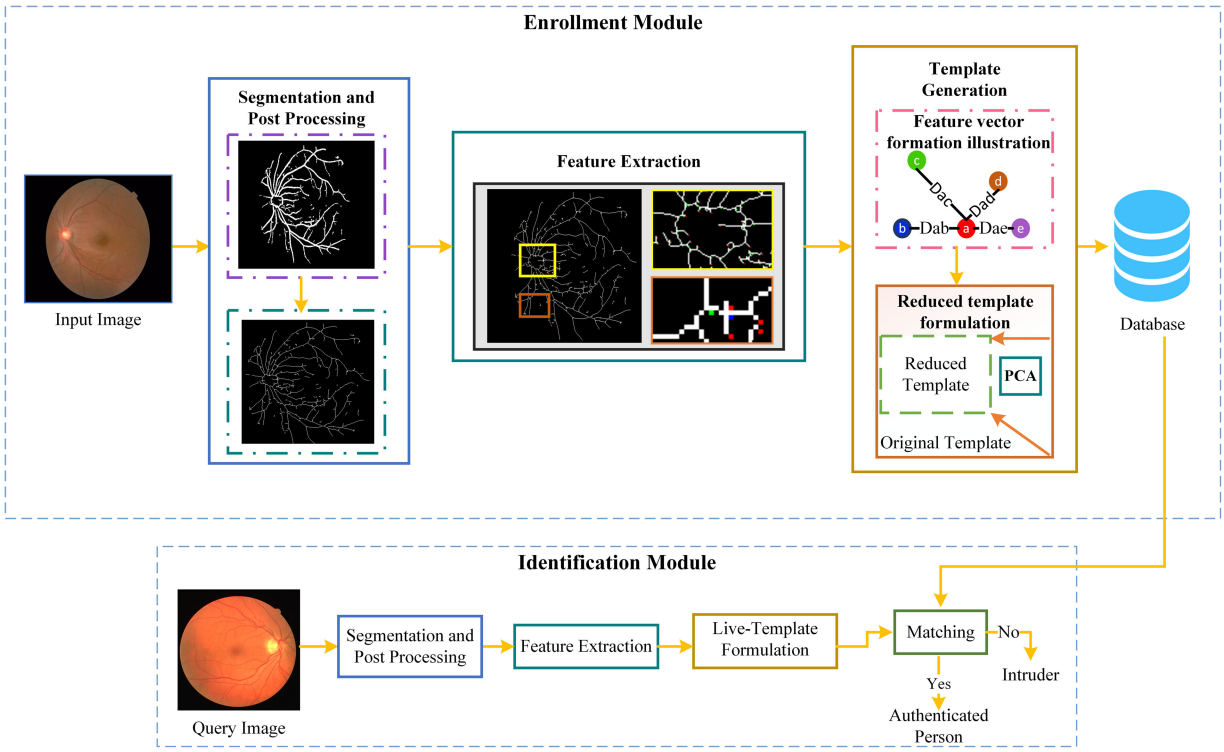

Fig. 2. Overview of the proposed approach. Enrollment and identification are two main modules. Enrollment module includes (1) Segmentation and postprocessing: The result of the final segmentation and skeletonization is shown. (2) Feature extraction: Features are extracted and highlighted using color slicing. Zoomed images depict the result of color slicing. (3) Template generation: Feature vector formation illustration: "a" is the candidate feature point. Distance and angle between "a" and its four nearest feature points "b," "c," "d," and "e" are found to formulate feature vector. (4) Reduced template formulation: PCA is applied for dimensionality reduction. The reduced template is then stored in the database. Identification module includes (1) Live-template formulation: Query image template (live-template) is generated. (2) Matching: L2-norm is used to find the distance between live-template and templates stored in the database. Depending on the distance, TSM is calculated. Query image is given a status either authenticated or intruder based on TSM.

branch points are used to map the hash table for every image. Jiu *et al.* [27] used Gabor wavelet transform for the enhancement of vessels. The feature vector is formed by calculating distance and angle between four nearest neighbors of a feature point. Euclidean distance is used to test authentication.

III. Enrollment Module

A. Preprocessing

The presence of noise in retinal images can render them inappropriate for identification phase [28], [29]. Retinal images contain nonuniform illuminations, blurry areas, and noisy background. Noise seems to be present in regions with poor illumination and is more prominent closer to retinal edges [30], [31]. Eye movements cause motion artifacts that induce blurring in images. Noise can also be induced by image acquisition modality, i.e., fundus camera [32]. Thus, preprocessing is used for artifacts exclusion and to make images appropriate for reliable feature extraction. Preprocessing is of vital significance as the overall strength of retinal identification depends on the final segmented image. To deal with variations of different datasets, standardization is done to make our technique universal for all datasets. Through experiments, the resolution of 256×256 is found to be optimal for performance. All images are resized to the resolution of 256×256.

1) Contrast Enhancement (CE): Green channel contains fine details and valuable information. Thus, to obtain maximum contrast between the blood vessels and background green channel is extracted. To make intensity uniform and to remove nonuniform illuminations from the images, Contrast Limited Adaptive Histogram Equalization (CLAHE) [33] is applied. CLAHE divides the image into nonoverlapping regions termed as tiles. Contrary to conventional CE methods, it prevents overamplification of noise by using a predefined value termed as clip limit [33]. There is no need for adaptive selection of CLAHE parameters because image size has been fixed to the resolution of 256×256. To select an appropriate clip limit for CLAHE, we varied clip limit from 0.01–0.05. With a clip limit of 0.01, the image quality was improved, the noise level was low and blood vessels were perceivable as well. To select tile size, we varied it from $[8 \times 8]$ to $[64 \times 64]$ and compared corresponding processing time. With different images, a window size of $[8 \times 8]$ had the least processing time. So for experiments, a clip limit of 0.01 and window size of $[8 \times 8]$ are applied to the extracted green channel (I_{gchannel}) for optimum performance.

2) Nonvascular Components Removal (NVCR): Segmentation process is accelerated by removing nonvascular components (NVC). NVC constitute of background, optic disc, macula, and other abnormalities. If NVC are not removed, the processing time will be more, blood vessels will not be enhanced appropriately, the noise will be more apparent, there will be nonuniform

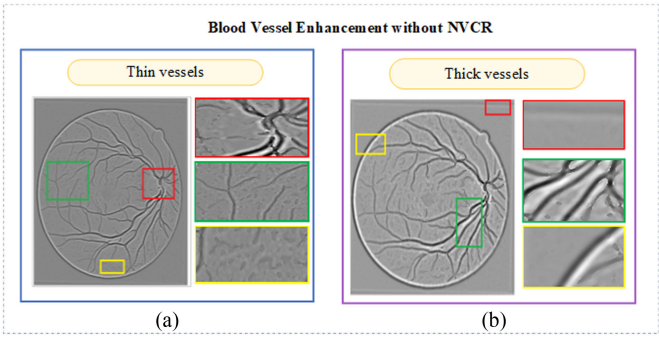

Fig. 3. (a) Thin vasculature obtained without using NVCR: Zoomed images show artifacts. Red = optic disc boundary is apparent, Green = blood vessels are not enhanced properly and somewhat suppressed, Yellow = noise is also present and has a similar texture to that of vessels. (b) Thick vasculature obtained without using NVCR. Red = nonuniform background, Green = illumination is present around blood vessels, Yellow = retinal boundary is also highlighted and there is no distinction between foreground and background.

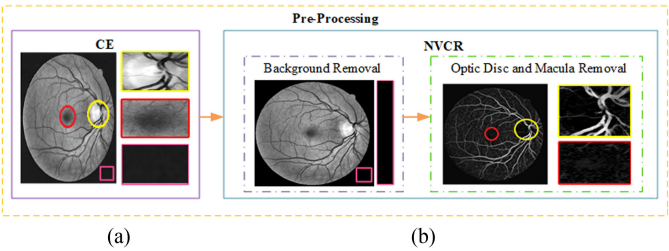

Fig. 4. Preprocessing. (a) CE module: Enhanced image obtained by applying CLAHE on I_{gchannel}. Zoomed images show NVC. Yellow = optic disc, Red = macula, Pink = background with noise. (b) NVCR module. Background removal: Removes the artifacts and noise in the background by masking enhanced image with mask. Zoomed image shows a complete black background with no noise. Optic disc and macula removal: Modified top-hat transform is applied for removing optic disc and macula.

background, the computational cost of successive methods will be more and NVC will appear as false positive during segmentation stage. These artifacts are clearly visible in Fig. 3. All these factors result in declined performance. Thus, NVCR has a crucial role in handling the general performance of the proposed system.

The region of interest (ROI) in retinal images corresponds to the semicircular region over a dark background [30]. The background is not actually black, but it contains noise [34]. Thus, it is necessary to mask the pixels that do not constitute ROI. Mask image is created by a two-stage process: coarse level and fine level. At the coarse level, Otsu threshold algorithm [35] is applied to I_{gchannel}. However, some pixels are misclassified at this stage. At the fine level, these pixels are classified correctly by morphological opening and closing operation with a disc-shaped structuring element having radius 2. After that, masking of I_{gchannel} is performed with the mask obtained. This step removes background noise and unwanted pixels that do not constitute ROI as shown in Fig. 4. Instead of a normal top-hat transform which induces noise, modified top-hat transform [36] is adopted. Modified top-hat ensures better noise removal and

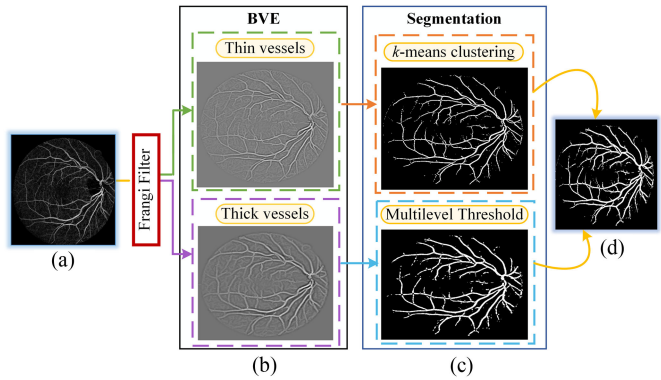

Fig. 5. Flow diagram showing blood vessels enhancement (BVE), segmentation, and image fusion. (a) Preprocessed image. (b) BVE module: Application of Frangi filter generated two outputs (Thin vessels network and thick vessels network). (c) Segmentation module: k-means clustering used for thin vessels network and multilevel thresholding used for thick vessels network. (d) Image fusion: Final segmented image obtained by fusion of thick and thin vessels.

suitable feature extraction

$$I_{\text{Tophat}} = I - (I \bullet S_c) \quad o \quad S_o \tag{1}$$

where I is input image, $\bullet$ is a closing operator, o is an opening operator, S_c is the structuring element used for closing, and S_o is the structuring element for opening, I_{Tophat} is the output image. For both closing and opening disk-type structuring element with the radius of 15 pixels is used. The opening stage of the modified top-hat transform removes the optic disc. Fig. 4(a) has the clear optic disc, macula, and noisy background. Proposed NVCR completely removes these NVC without effecting the blood vessels in the optic disc region as shown in Fig. 4(b).

3) Blood Vessels Enhancement: Without BVE, the output generated by NVCR will be directly subjected to the segmentation module. It is clearly evident from Fig. 4(b) that the output of NVCR is not appropriate for vasculature segmentation. It needs proper enhancement before segmentation. Hence, BVE is a crucial factor for blood vasculature enhancement and to make image appropriate for segmentation. Currently used enhancement techniques also enhance the noise that appears as spurs in the segmented result and increases false positive rate. Frangi filter is used in this paper for BVE. Contrary to existing techniques that enhance whole structure, Frangi filter performs enhancement of only elongated structures. In the case of retinal images, these structures constitute blood vessels. Thus, the noise is suppressed as shown in Fig. 5(b). Given a continuous 2-D image $I(\hat{Y})$, Frangi filter [37] for blood vessel enhancement is adopted

$$r(\hat{Y}, \sigma, \beta_1, \beta_2) = \begin{cases} 0 & \text{if } \lambda_2(\hat{Y}, \sigma) > 0 \\ \exp\left(-\frac{R_B^2(\hat{Y},\sigma)}{2\beta_1^2}\right) \times & \\ \left(1 - \exp\left(-\frac{S^2(\hat{Y},\sigma)}{2\beta_2^2}\right)\right), & \text{otherwise} \end{cases} \tag{2}$$

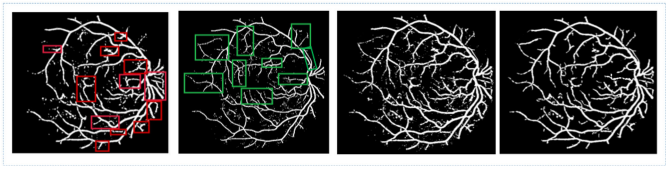

Fig. 6. (a) Vasculature estimated by multilevel Otsu threshold. The highlighted portion is estimated by multilevel threshold. (b) Vasculature estimated by k-means. The highlighted portion is estimated only by k-means. (c) Image fusion: combines and harness results of (a) and (b) to create a single-fused image (I_{fused}). I_{fused} is more informative, as it combines information from both (a) and (b). (d) Postprocessing: Result obtained by performing area opening of I_{fused}.

where $\lambda_1(\hat{Y},\sigma)$ and $\lambda_2(\hat{Y},\sigma)$ are eigenvalues of local Hessian estimated at $\hat{Y}$ with scale σ. $R_B(\hat{Y},\lambda) = \frac{\lambda_1(\hat{Y},\sigma)}{\lambda_2(\hat{Y},\sigma)}$ is the elongated strength. It calculates the variation from blob by taking into account the eccentricity of the second ellipse. The structureness measure is given by $S(\hat{Y},\sigma) = \sqrt{\lambda_1^2(\hat{Y},\sigma) + \lambda_2^2(\hat{Y},\sigma)}$. The parameters β_1 (Frangi beta one) and β_2 (Frangi beta two) control sensitivity of the filter to deviation in $R_\beta(\hat{Y},\sigma)$ and $S(\hat{Y},\sigma)$ [38]. The values used for β_1 and β_2 are 2 and 3.5.

B. Segmentation

Segmentation is a paramount of overall performance because the errors prevailing in final segmented retinal image will significantly affect the feature extraction and identification process. In phase-based level set methods, vessel width plays an important role in the wavelet response. Thick blood vessels give a high response in contrast to thin vessels [17]. Due to varying wavelet response, thin vessels may get discarded. Another overhead of such methods is the optimal threshold selection to handle varying wavelet response. To overcome these issues and to retain both thick and thin vessels, hybrid segmentation technique is used. The proposed hybrid segmentation approach effectively balances the difference of wavelet response between thick/thin blood vessels. The use of hybrid segmentation is more effective to retain as much vasculature as possible and also prevents thin vessels from being discarded. As a result, recognition accuracy is improved. The advantage and contribution of hybrid segmentation are evident from Fig. 6. k-means clustering is used for thin vessels segmentation. k-means is a data clustering iterative algorithm that partitions the data points into clusters on the basis of their distances from the centroid [39]. To choose clusters k optimal for our dataset, average silhouette method [40], [41] is used. Multilevel thresholding using Otsu is used for thick blood vessels segmentation. It performs well where the image has to be divided into two classes of pixels. It automatically calculates the optimum threshold in such a way that it maximizes between class variance of segmented classes [35].

After segmentation, image fusion is performed to harness the results generated by k-means and multilevel threshold to generate a single-fused image. Image fusion is performed by spatial domain fusion method. We particularly used pixel-level fusion using the maximum method from spatial domain [42]. The maximum method performs a selection process. Every corresponding pixel of the images to be fused is compared. After that, the pixel with the maximum intensity is selected and placed on the corresponding position of the resultant image

$$I_{\text{fused}}(i,j) = \sum_{i=1}^{M}\sum_{j=1}^{N} \max(X_1(i,j), X_2(i,j), \ldots, X_n(i,j)) \tag{3}$$

where $X_1, X_2, \ldots, X_n$ are the input images, I_{fused} is the output fused image, n is the total number of images to be fused, $\max()$ finds the maximum intensity pixel, and M and N correspond to the total number of rows and columns. The reason for opting out this particular method is that it does not compromise over the good information available in the image, it is fast and efficient. Its disadvantage is that the maximum pixel is not always the better pixel. However, it is rectified in our method by postprocessing. As evident from Fig. 6(c), I_{fused} is more informative as compared to results generated by the individual segmentation. As proposed segmentation retains both vessels, so it outperforms the other existing segmentation techniques and have high accuracy.

C. Postprocessing

Before analyzing I_{fused} for identification, it is subjected to postprocessing to get rid of spurs and unwanted regions produced during segmentation. Area opening is used to remove these artifacts. In this paper, vessels that have less than or equal to 20 pixels are regarded as unwanted regions and are discarded out. The result of area opening is shown in Fig. 6(d). Before feature extraction, it is necessary to reduce vessels width to 1. Without width reduction, the feature extraction stage will yield incorrect features as evident from Fig. 7(a). Width is reduced by skeletonization. For skeletonization, MATLAB's built-in morphological function named $bwmorph$ is used [43]. $I_{\text{skel}} = bwmorph(bw,' skel', Inf)$ where bw is the segmented image obtained after area opening, with Inf $bwmorph$ repeats the operation until there is no further change in the image. Fig. 7 shows a stepwise illustration of feature extraction performed with and without skeletonization.

D. Feature Extraction

Like other biometric identification systems, retinal identification also relies on its unique features to distinguish subjects from one another. These include end point (end of a vessel), bifurcation (where a vessel splits into two), and crossing over (the point where two vessels meet up) as shown in Fig. 1. To ensure maximum discriminant power and high accuracy, we used all three of them. For feature extraction, crossing number technique is used. It takes the skeleton image I_{skel} as input and outputs an image with extracted features F (see Fig. 7)

$$\text{CN}(P) = \frac{1}{2}\sum_{i=1}^{8} |I_{\text{skel}}(p_i) - I_{\text{skel}}(p_{i+1})| \tag{4}$$

where P is the pixel to be evaluated, p_i are the pixels surrounding P in a clockwise direction, and I_{skel} is the skeleton image. CN is half of the sum of the difference between adjacent pixels in the

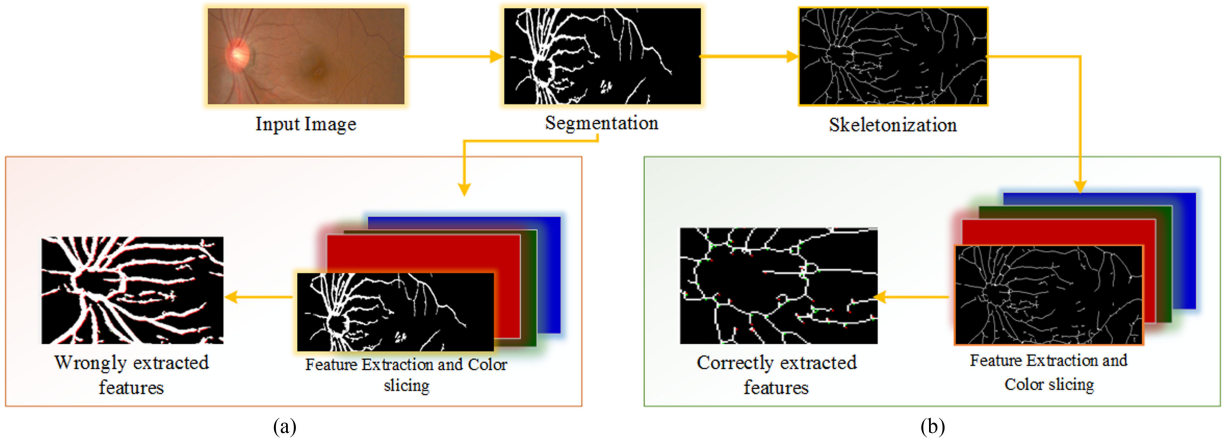

Fig. 7. Two possible outcomes of the feature extraction phase. (a) Result of feature extraction performed without skeletonization. Consequently, the feature extraction generates wrong features. (b) Result of feature extraction performed with skeletonization. The extracted features are correct and each one is marked correctly by color slicing.

Algorithm 1: Feature Extraction and Color Slicing.

Require: Skeleton Image I_{skel}
Ensure: Final Image with extracted features F
Do zero padding of I_{skel} to obtain a matrix img;
Initialize a matrix Clr_Img (with three layers) having the same size as that of I_{skel} for color slicing;
for $\forall\, p \in$ img **do**
  if img$[p] == 1$ **then**
    Calculate CN value using (4);
    Color Slicing: Evaluate computed CN value;
    if CN $== 1$ **then**
      p is end point;
      $Clr\_Img\,[p] \leftarrow$ Red Color;
    else if CN $== 3$ **then**
      p is bifurcation;
      $Clr\_Img\,[p] \leftarrow$ Green Color;
    else if $CN > 3$ **then**
      p is crossing over;
      $Clr\_Img\,[p] \leftarrow$ Blue Color;
    end if
  else
    Move to img$_{(p+1)}$;
  end if
end for
$N\_\text{Img} = \text{cat}(3, I_{\text{skel}}, I_{\text{skel}}, I_{\text{skel}})$;
$F = N\_Img + Clr\_img$;

8-neighborhood of P. Algorithm 1 is the pseudocode for crossing number and color slicing. CN explores 8-neighborhood of a pixel that constitutes vessel in a clockwise direction. Depending on final CN value, a pixel is designated as one of the feature point. Color slicing is used to highlight the detected feature points. For color slicing, a matrix with three layers (Clr_img) having the same dimension as that of I_{skel} is initialized. Corresponding to CN value, a specific color (Red for end point, Green for bifurcation, Blue for crossing over) is stored at the same location in Clr_img. Once feature extraction is completed, Clr_img is superimposed on I_{skel}. Before superimposition, I_{skel} is also concatenated in three dimensions to have an image with three layers (N_{Img}). Superimposition of Clr_{img} on N_{Img} gives the final image F with all extracted features highlighted as shown in Fig. 7(b).

E. Template Generation

1) Template Formulation: Once features are extracted, the next step is to formulate the templates and store them in the database. The matching phase is paramount for the identification process. Irrespective of rotation and translation, the angle and distance between different feature points remain the same. This consistency is harnessed to ensure that matching is rotation and translation invariant. The angle and distance between a candidate feature point and its four nearest feature points are calculated to formulate a template. Resulting template is of dimension $R \times 8$, where R is the number of features and varies for every image.

2) Dimensionality Reduction: The massive number of templates in the database and the type of templates require much time to compare query images. It slows down the matching process and makes it more complex. Feature extraction phase yields templates of varying dimensionality. Most of the existing retinal identification techniques focused only on accuracy and not on time efficiency. To make proposed matching process time efficient, it is hastened by reducing template dimensionality. The proposed approach used PCA-based feature processing approach for efficiently reducing the dimensionality of a large number of vessels features. PCA is used because it converts the set of features into a reduced number of uncorrelated features. PCA ensures that principal components not only correspond to maximum variance, but also ensures that resulting set of features in the subspace are uncorrelated while retaining most of the information content [47], [48]. This guaranteed uncorrelation improves the predictive performance of resulting features. The enhanced predictive power improves the performance of the classifier.

The new retinal features are termed as retinal Eigen features. Every original retinal feature is transformed into an Eigen value. First, every image is converted into a column vector and stacked into a matrix, i.e., $M = \{M_1, M_2, \ldots, M_N\}$. The zero-mean vector of each vector is found by subtracting the vector from mean

$$x_0 = \frac{1}{N}\sum_{i=1}^{N} M_i - \bar{x} \rightarrow \bar{x} = \sum_{i=1}^{N} x_i/N \tag{5}$$

where x_0 is zero-mean vector, M_i is ith column vector in matrix M, x_i is ith entry in the vector M, $\bar{x}$ is mean, and $i = 1, \ldots, N$. After mean, covariance matrix is computed as

$$C = (x_0)(x_0)^T \tag{6}$$

where C is the covariance matrix, x_0 is zero mean vector, T is transpose, and x_0^T is the transpose of zero mean vector. As C is large dimensionality matrix, Eigen vectors are calculated to obtain distinguishing features and remove redundant ones as

$$C_v = \lambda E_v \tag{7}$$

where λ is Eigen value, E_v is Eigen vector, and C_v is the matrix associated with Eigen values λ of vector E_v. All the images are transformed to Eigen subspace as

$$y = W^T(M_i) \qquad i = \{1, 2, \ldots, N\} \tag{8}$$

where y is Eigen subspace termed as principal components or retinal Eigen features, W is projection matrix constructed from selected Eigen vectors, T is transpose, and W^T is transpose of projection matrix. The first N Eigen features with high variance are selected. As a result, dimensionality is reduced. The resulting retinal Eigen features are stored in the database.

Without PCA, all templates will have varying dimension. With the massive number and template size, identification will take more time and will be inappropriate for real-time applications. PCA significantly reduced the dimension of the templates. The time interval between matching and identification process is reduced. Consequently, the proposed technique takes less time in matching and is computationally more efficient. The statistical details of time efficiency achieved by the proposed technique are discussed later in Section V-A.

IV. Identification Module

When an unknown subject sample is given, the system generates its live-template. L2-norm is used to calculate the feature distance between the feature vector of live-template and the feature vector of all the templates stored in the database

$$||v|| = \sqrt{\sum_{i=1}^{k} |v_i^2|} \tag{9}$$

where v is a vector, k is the total number of elements in vector v, and $|v_i^2|$ is absolute of squared values in v. To evaluate the similarity between samples, TSM is calculated. Whenever the live-template feature vector has minimum feature distance with some stored template feature vector, the TSM for that subject is incremented by 1. TSM is calculated as

$$\text{TSM} = \text{Subject ID}[\text{find}(\min_i(\text{FD}))] + 1, i = 1, \ldots, N \tag{10}$$

where find() is a function for seeking index position, min() is a function that returns the minimum element, FD is the feature distance, Subject ID is an array having the same length as that of the number of subjects in the database and is used for storing the matching score, N is the total number of templates stored in the database. find(min(FD)) finds the index position where the minimum value of FD is encountered. After that, an increment of TSM is done to that index of the Subject ID. The result of this matching is a list of TSM values. After the live template has been compared with all the templates in the database the final decision is made by comparing maximum TSM with a threshold as

$$\max(\text{TSM}) \geq T \tag{11}$$

where T is the threshold. If the above condition is satisfied, then the query image is regarded as authenticated. Otherwise, it is rejected as an intruder. Thresholding step is vital for rejection of intruders.

V. Experimental Results

The algorithm is implemented and tested using MATLAB R2015b environment on a workstation with Intel(R) CORE(TM) i3-4130, 3.40 GHz, and 8 GB RAM. In contrast to face recognition, very few databases are available for retinal identification. To the best of our knowledge, VARIA [50] and RIDB [51] are the only publicly available databases for retinal identification purpose. For this reason, we created our own database named BRDB. Other existing techniques have evaluated performance on some local database or on publicly available databases like DRIVE [52] and STARE [44]. Local databases are not publicly available. Hence for a fair comparison with these techniques and to make publicly available databases suitable for identification, augmentation is used to generate multi-samples per subject. Each image is rotated randomly to generate nine samples per subject. For performance evaluation on pathological images STARE [44], DIARETDB0 [45], Messidor [46], and HRF [49] are used. Experimental section is further divided into two sections: Retinal Identification and Retinal Vasculature Segmentation.

A. Retinal Identification

Proposed approach authenticity is evaluated by conducting different experiments. A personal database BRDB is designed to evaluate the validity of the proposed technique. BRDB consists of 1800 color retinal images of 200 subjects with nine samples per subject. Images are captured using Fundus camera TOPCON TRC NW300, having 8M pixels per inch (PPI), and are nonmydriatic with a 45° field of view. The images are macular centered, have the dimension of $(1536 \times 2048 \times 3)$, and are stored in .JPG format. To evaluate proposed technique performance, 60 subjects were selected to act as authenticated users. Out of nine samples, six samples are used for training, and three samples are used for testing. 70 subjects were

TABLE I
PERFORMANCE COMPARISON FOR RETINAL IDENTIFICATION

No.	Method	Database	Total Images	Correctly Recognized	Wrongly Recognized	Accuracy %	Identification Rate%
1	Akram et al. [16]	DRIVE STARE VARIA	40 81 233	40 77 231	0 4 2	100 95.05 99.14	98.30
2	Hussain et al. [18]	DRIVE	40	39	1	97.50	97.50
3	Sadikoglu and Uzelaltinbulat [21]	DRIVE	-	-	1	97.50	97.50
4	Qamber et al. [4]	DRIVE STARE VARIA	40 81 233	40 78 232	0 3 1	100 96.29 99.57	98.87
5	Monisha and Seldevchristopher [24]	DRIVE STARE	40 100	39 97	1 3	97.5 97	98.87
6	Sabaghi et al. [23]	DRIVE	40	40	0	100	100
7	Jiu et al. [27]	DRIVE STARE VARIA	- - -	- - -	- - -	100 95.06 98.28	97.78
8	Fatima et al. [17]	VARIA RIDB	233 100	232 97	1 3	99.57 97	98.28
9	Farzin et al. [19]	DRIVE+STARE	300	-	-	99.0	99.0
10	Köse et al. [22]	STARE	80	-	-	95.0	95.0
11	**Our Proposed**	DRIVE STARE VARIA RIDB **Our BRDB**	40 81 233 100 1800	40 81 232 98 1797	0 0 1 2 3	100 100 99.57 98 99.46	99.40*

* Other techniques have only used DRIVE, STARE, VARIA, or RIDB. Due to this in some cases, their average identification rate is more as compared to our proposed technique. In contrast, our method is evaluated on all of them including BRDB. The proposed method achieved the highest accuracy databasewise.

TABLE II
PERFORMANCE ON IMAGES WITH DEGENERATIONS

Database	Total Images	Correctly Recognized	Wrongly Recognized	Identification Rate (%)
STARE [46]	400	399	1	99.75
HRF [52]	45	45	0	100
Messidor [48]	800	797	3	99.62
DIARETDB0 [47]	130	128	2	98.46

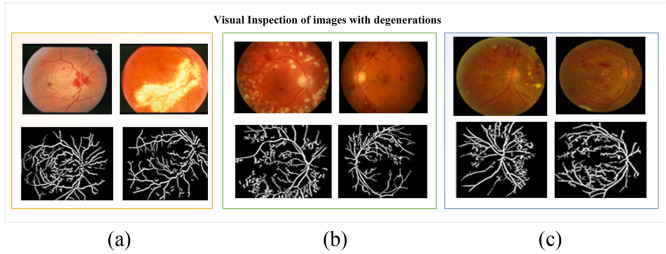

Fig. 8. Performance of our method on images with large degenerations. The first row corresponds to input images. The second row corresponds to the result of segmentation achieved by our method. (a) Images from STARE [44]. (b) Images from DIARETDB0 [45]. (c) Images from Messidor [46].

selected to act as intruders. This setup created a total of 810 experiments ($60 \times 3 = 180$ authenticated subjects experiment, $70 \times 9 = 630$ intruder experiments). The proposed approach achieves the highest recognition rate that makes it more effective. It outperforms other existing techniques as clearly evident from Table I. For pathological cases, effectiveness of technique is evaluated using STARE [44], DIARETDB0 [45], Messidor [46] (first two sets), and HRF [49]. The statistical results of performance with these databases are given in Table II. It is evident that the proposed technique achieves a high identification rate even with these databases. Fig. 8 shows the visual results obtained with these databases. The results clearly depict proposed technique strength to deal with images having degenerations. The proposed approach is further validated by false acceptance rate (FAR), false rejection rate (FRR), and equal error rate (EER). These matrices vary according to the chosen threshold. There is always a tradeoff between FAR and FRR. Fig. 9 shows the effect on FAR and FRR with respect to change in threshold values. The intersection point of FAR and FRR represents EER. From Fig. 9(c), it is clear that our method achieves an EER of zero which makes it completely accurate and gives it a lead over existing techniques.

1) Identification Time: Biometric systems have to be used in real time, so they must be computationally accelerated and time efficient. Our method achieved this acceleration by using PCA. PCA reduced dimensionality and decreased the time interval between matching and identification process. The

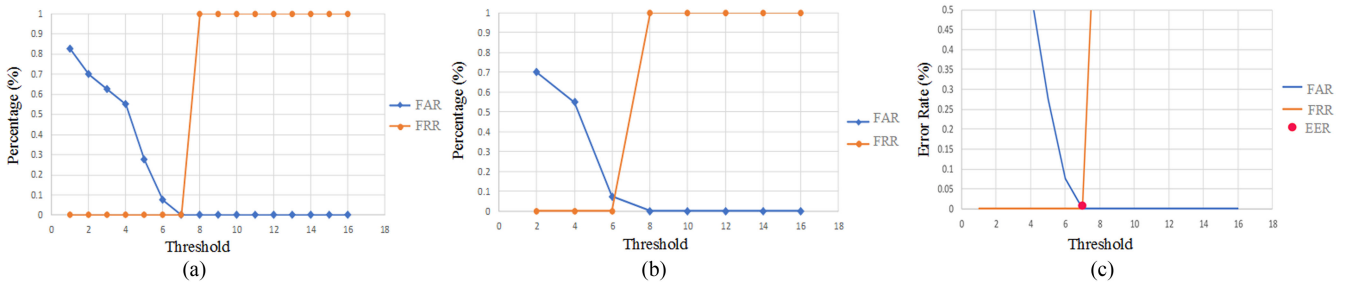

Fig. 9. FAR and FRR curves for retinal identification. (a) and (b) show the dependence of FAR and FRR on the threshold. (c) FAR and FRR with respect to the error rate. The intersection point represents EER, which is demonstrated by a magenta circle. As our approach has EER = "0," thus it is accurate.

TABLE III
IDENTIFICATION TIME COMPARISON WITH/WITHOUT PCA

Database	Total Images	Query Image Name	Total Identification Time (sec)	
			Without PCA	With PCA
DRIVE [51]	40	38_training.tif	523.19	0.019
STARE [46]	100	Im0038.ppm	821.77	0.037
VARIA [49]	233	012.pgm	930.28	0.086
HRF [52]	45	08_h.jpg	529.27	0.024
Our BRDB	1800	4.jpg	827.20	0.029
Average Time	-	-	736.342	**0.039**

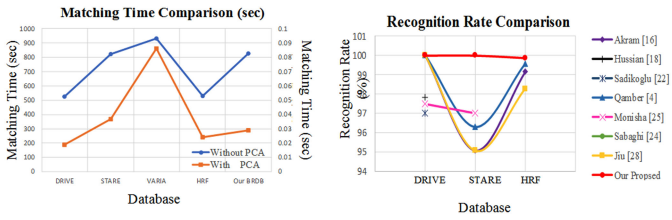

Fig. 10. (a) Identification time comparison with and without PCA. Our approach has significantly accelerated the matching. (b) Recognition rate comparison of different techniques. Our approach has the highest recognition rate.

statistical details of time efficiency achieved by the proposed technique is given in Table III. The identification time for the techniques without any acceleration ranges from 500–900 s. On the other hand, the proposed technique significantly reduced it to a range of 0.019–0.029 s. Average time clearly shows that the proposed approach is much more efficient. This efficiency makes the proposed method more appropriate for real-time applications. Fig. 10(a) shows acceleration achieved by the proposed method as compared to techniques without any acceleration mechanism. Thus, experimental results showed our method has low computational time and outperforms techniques without any acceleration mechanism. The total identification time comprises of a fixed time (required for retinal image preprocessing, segmentation, and feature extraction) and a variable time for the one-to-many matching process. Total identification time is calculated as

$$\text{Total\_identification\_time} = \text{Fixed Time} + TL(\text{one-to-one template matching}) \quad (12)$$

where TL is the total number of templates stored during registration, Fixed Time is 0.316 s, and one-to-one template matching time is 0.0079 s (on a workstation with Intel(R) CORE(TM) i3-4130, 3.40 GHz, and 8 GB RAM).

2) Feature Comparison: Selected features discriminant power is evaluated by comparing it with different kinds of features (end points, bifurcations, and proposed combination of end points, bifurcations, and crossing over). Performance of all these features is evaluated and compared by the following experiment. FD between the live template of different subjects and registered subjects is calculated. If the template belongs to the same class, then distance is categorized as in-class. Otherwise, the distance is categorized as between-class. The distribution of the two distances is approximated as histograms. Intuitively, if a feature has good discrimination power, then there will be no overlapping between both kinds of distances and there will be a clear distinction among classes. The histograms obtained as a result of this experiment are shown in Fig. 11. When end points and bifurcations are used independently, there is an overlapping of between-class and in-class distance. With our combination, there is no overlap and a clear discriminant boundary among classes. Hence, the identification phase leads to correct results with high accuracy.

3) Impact of Scaling on System Performance: The impact of scaling has been analyzed in terms of execution time, identification rate, and an average number of extracted features as shown in Fig. 12. For analyzing the impact of scaling on system performance, we downsampled the images from the original resolution. The images are resampled to the resolutions of 512×512, 256×256, 128×128, 64×64, 32×32, and 16×16, respectively. Fig. 12(c) shows that the identification rate with the resolution of 512×512 and 256×256 is the same. However, the execution time with the resolution of 256×256 is faster as compared to the resolution of 512×512. With the resolution of 16×16 execution time is fastest, but the identification rate declines to 65%. So for the optimal performance, all the images are downsampled to the resolution of 256×256. With the increase in image size, the number of extracted feature increases correspondingly. However, with the increased number of extracted features execution time increases, the identification becomes slow.

B. Retinal Vasculature Segmentation

To evaluate proposed technique performance for segmentation, it has been validated on DRIVE [52], STARE [44], and has been compared with other existing techniques. The

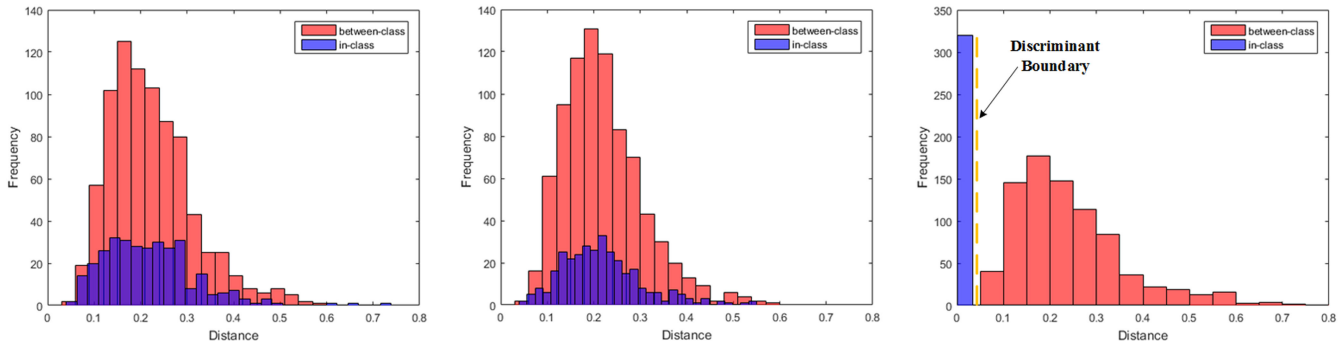

Fig. 11. Discriminant power comparison. (a) End points as feature points. (b) Bifurcation as feature points. Clearly, in both (a) and (b), there is overlapping of in-class and between-classes distances. Thus, subjects are not identified correctly. (c) Proposed combination of features points. There is no overlapping and there is a clear discriminant boundary among classes.

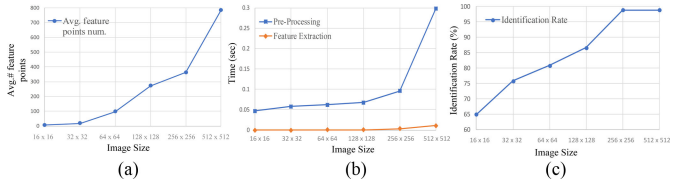

Fig. 12. (a) Scaling effect on average feature points number. (b) Scaling effect on time consumed in preprocessing and features extraction. (c) Scaling effect on identification accuracy.

TABLE IV
COMPARISON FOR RETINAL VASCULATURE SEGMENTATION

Method	DRIVE			STARE		
	Acc	Sn	Sp	Acc	Sn	Sp
Staal et al. [51]	0.944	0.719	0.977	0.952	0.697	0.981
You et al. [53]	0.943	0.741	0.975	0.950	0.726	0.976
Soares et al. [54]	0.946	0.724	0.976	0.948	0.710	0.974
Singh and Srivastava [55]	0.952	0.759	0.971	0.927	0.794	0.938
Imani et al. [56]	0.952	0.752	0.975	0.959	0.750	0.975
Vlachos and Dermatas [57]	0.929	0.747	0.955	-	-	-
BahadarKhan et al. [58]	0.961	0.746	0.980	0.946	0.758	0.963
Our Proposed	0.968	0.756	0.978	0.963	0.755	0.963

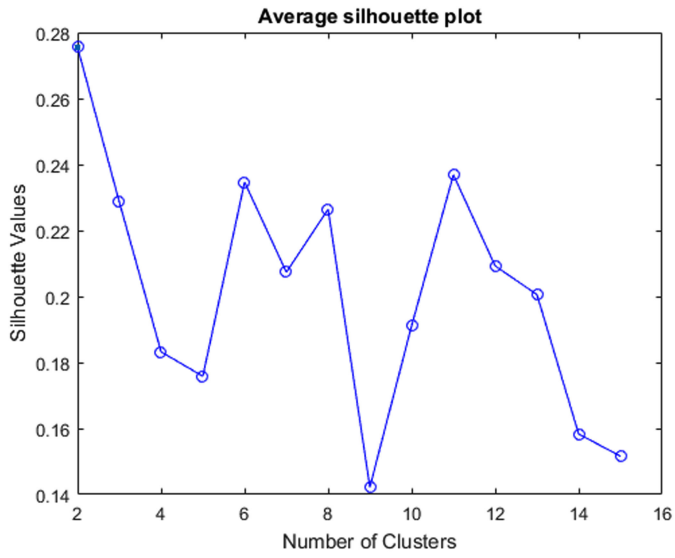

Fig. 13. Average silhouette plot for computing k. The plot peak value is 2. Thus, $k = 2$ is proper cluster choice.

performance is evaluated with respect to three evaluation measures, i.e., Accuracy (Acc), Sensitivity (Sn), and Specificity (Sp). The statistical results of this comparison are given in Table IV. The proposed segmentation is very efficient and achieved the highest accuracy as compared to all other paralleled techniques. Our method also achieved highest Sn and Sp for DRIVE except for Singh and Srivastava [55] and Khan *et al.* [58], which is only better comparatively by a difference of 0.003 and 0.002. While in the case of STARE, Sn of Singh and Srivastava [55] and Khan *et al.* [58] are 0.039 and 0.003 better. The Sp of You [53], Soares [54], and Imani are slightly better by 0.013, 0.011, and 0.012, respectively. Fig. 8 shows the effectiveness of our segmentation technique. The experimental results validate that the suggested method is very effective as compared to other cited frameworks. To choose the number of clusters (k) of k-means clustering that are optimal for segmentation of our dataset, average silhouette method [40], [41] is used. We computed k-means clustering by varying k from 1–15. For each k, the average silhouette of observations is then calculated. The maximum location of average silhouette plot is considered as the appropriate number of clusters [40], [41]. As evident from Fig. 13, the maximum location of average silhouette plot for our dataset is observed at 2. Thus, the value of k is set to 2.

VI. CONCLUSION

An automatic fast and accurate retinal identification system with hybrid vasculature extraction is developed for the large-scale multisample retinal dataset. In contrast to other techniques, high recognition accuracy is achieved by using a hybrid segmentation technique. Experimental results showed an identification rate of 99.40% with the EER of zero. The proposed hybrid segmentation effectively balances the difference of wavelet response between thick/thin blood vessels. It achieved an accuracy of 99.6%. PCA-based feature processing approach significantly reduced the computation time and accelerated the matching process. Our approach has low computational time and is computationally more efficient. The limitation of this paper is that

with images having severe pathological noise the identification rate is low as compared to normal images. The reason for this decline is that in presence of severe pathological disorder it is difficult to extract the feature points. Due to this difficulty, another limitation arises, i.e., identification time for such images is more as compared to normal ones. In the future, we will overcome this limitation by particularly improving our image enhancement module. Improved image enhancement will yield more enhanced images for pathological cases as well. That, in turn, will aid the feature extraction phase. This convenient feature extraction will make the identification process fast for pathological cases as well. Alongside we plan to create an even more larger retinal database, with images taken over even much longer periods and improve performance by applying various discriminant analytics.

REFERENCES

[1] M. Wazid, A. K. Das, N. Kumar, and J. J. P. C. Rodrigues, "Secure three-factor user authentication scheme for renewable-energy-based smart grid environment," *IEEE Trans. Ind. Informat.*, vol. 13, no. 6, pp. 3144–3153, Dec. 2017.

[2] F. Zhao, H. Luo, X. Zhao, Z. Pang, and H. Park, "HYFI: Hybrid floor identification based on wireless fingerprinting and barometric pressure," *IEEE Trans. Ind. Informat.*, vol. 13, no. 1, pp. 330–341, Feb. 2017.

[3] P. Hu, H. Ning, T. Qiu, Y. Zhang, and X. Luo, "Fog computing based face identification and resolution scheme in internet of things," *IEEE Trans. Ind. Informat.*, vol. 13, no. 4, pp. 1910–1920, Aug. 2017.

[4] S. Qamber, Z. Waheed, and M. U. Akram, "Personal identification system based on vascular pattern of human retina," in *Proc. Cairo Int. Biomed. Eng. Conf.*, 2012, pp. 64–67.

[5] Z. Chen, Q. Zhu, Y. C. Soh, and L. Zhang, "Robust human activity recognition using smartphone sensors via CT-PCA and online SVM," *IEEE Trans. Ind. Informat.*, vol. 13, no. 6, pp. 3070–3080, Dec. 2017.

[6] K. Zinchenko, C.-Y. Wu, and K.-T. Song, "A study on speech recognition control for a surgical robot," *IEEE Trans. Ind. Informat.*, vol. 13, no. 2, pp. 607–615, Apr. 2017.

[7] A. K. Jain, A. Ross, and S. Pankanti, "Biometrics: A tool for information security," *IEEE Trans. Inf. Forensics Security*, vol. 1, no. 2, pp. 125–143, Jun. 2006.

[8] Z. Chen, L. Zhang, Z. Cao, and J. Guo, "Distilling the knowledge from handcrafted features for human activity recognition," *IEEE Trans. Ind. Informat.*, vol. 14, no. 10, pp. 4334–4342, Oct. 2018.

[9] V. S. Joshi, M. K. Garvin, J. M. Reinhardt, and M. D. Abramoff, "Identification and reconnection of interrupted vessels in retinal vessel segmentation," in *Proc. IEEE Int. Symp. Biomed. Imag., From Nano Macro*, 2011, pp. 1416–1420.

[10] S. Chaudhuri, S. Chatterjee, N. Katz, M. Nelson, and M. Goldbaum, "Detection of blood vessels in retinal images using two-dimensional matched filters," *IEEE Trans. Med. Imag.*, vol. 8, no. 3, pp. 263–269, Sep. 1989.

[11] Y. A. Tolias and S. M. Panas, "A fuzzy vessel tracking algorithm for retinal images based on fuzzy clustering," *IEEE Trans. Med. Imag.*, vol. 17, no. 2, pp. 263–273, Apr. 1998.

[12] X. Jiang and D. Mojon, "Adaptive local thresholding by verification-based multithreshold probing with application to vessel detection in retinal images," *IEEE Trans. Pattern Anal. Mach. Intell.*, vol. 25, no. 1, pp. 131–137, Jan. 2003.

[13] M. Sofka and C. V. Stewart, "Retinal vessel centerline extraction using multiscale matched filters, confidence and edge measures," *IEEE Trans. Med. Imag.*, vol. 25, no. 12, pp. 1531–1546, Dec. 2006.

[14] F. Zana and J.-C. Klein, "Segmentation of vessel-like patterns using mathematical morphology and curvature evaluation," *IEEE Trans. Image Process.*, vol. 10, no. 7, pp. 1010–1019, Jul. 2001.

[15] A. M. Mendonca and A. Campilho, "Segmentation of retinal blood vessels by combining the detection of centerlines and morphological reconstruction," *IEEE Trans. Med. Imag.*, vol. 25, no. 9, pp. 1200–1213, Sep. 2006.

[16] M. U. Akram, A. Tariq, and S. A. Khan, "Retinal recognition: Personal identification using blood vessels," in *Proc. Int. Conf. Int. Technol. Secured Trans.*, 2011, pp. 180–184.

[17] J. Fatima, A. M. Syed, and M. U. Akram, "A secure personal identification system based on human retina," in *Proc. IEEE Symp. Ind. Electron. Appl.*, 2013, pp. 90–95.

[18] A. Hussain, A. Bhuiyan, A. Mian, and K. Ramamohanarao, "Biometric security application for person authentication using retinal vessel feature," in *Proc. Int. Conf. Digital Image Comput., Techn. Appl.*, 2013, pp. 1–8.

[19] H. Farzin, H. Abrishami-Moghaddam, and M.-S. Moin, "A novel retinal identification system," *EURASIP J. Adv. Signal Process.*, vol. 2008, pp. 280 635:1–280 635:10, 2008.

[20] M. Womack, "The eyes have it," *Sensor Rev.*, vol. 14, no. 4, pp. 15–16, 1994.

[21] F. Sadikoglu and S. Uzelaltinbulat, "Biometric retina identification based on neural network," *Procedia Comput. Sci.*, vol. 102, pp. 26–33, 2016.

[22] C. Köse and C. İki *et al.*, "A personal identification system using retinal vasculature in retinal fundus images," *Expert Syst. With Appl.*, vol. 38, no. 11, pp. 13 670–13 681, 2011.

[23] M. Sabaghi, S. R. Hadianamrei, A. Zahedi, and M. N. Lahiji, "A new partitioning method in frequency analysis of the retinal images for human identification," *J. Signal Inf. Process.*, vol. 2, no. 4, pp. 274–278, 2011.

[24] L. S. Monisha and C. Seldevchristopher, "Biometric identification using retina scan," *Int. J. Adv. Res. Trends Eng. Technol.*, vol. 2, pp. 145–151, 2015.

[25] G. Sasidharan, "Retina based personal identification system using skeletonization and similarity transformation," *Int. J. Comput. Trends Technol.*, vol. 17, no. 3, pp. 144–147, 2014.

[26] M. A. El-Sayed, M. Hassaballah, and M. A. Abdel-Latif, "Identity verification of individuals based on retinal features using Gabor filters and SVM," *J. Signal Inf. Process.*, vol. 7, pp. 49–59, 2016.

[27] F. Jiu, K. Noronha, and D. Jayaswal, "Biometric identification through detection of retinal vasculature," in *Proc. IEEE Int. Conf. Power Electron., Intell. Control Energy Syst.*, 2016, pp. 1–5.

[28] J. Wei and G. Li, "Automated lung segmentation and image quality assessment for clinical 3-D/4-D-computed tomography," *IEEE J. Transl. Eng. Health Med.*, vol. 2, 2014, Art. no. 1800110.

[29] M. S. Haleem, L. Han, J. van Hemert, B. Li, and A. Fleming, "Retinal area detector from scanning laser ophthalmoscope (SLO) images for diagnosing retinal diseases," *IEEE J. Biomed. Health Informat.*, vol. 19, no. 4, pp. 1472–1482, Jul. 2015.

[30] A. Tariq and M. U. Akram, "An automated system for colored retinal image background and noise segmentation," in *Proc. IEEE Symp. Ind. Electron. Appl.*, 2010, pp. 423–427.

[31] N. P. Ward, S. Tomliivson, and C. J. Taylor, "Image analysis of fundus photographs: The detection and measurement of exudates associated with diabetic retinopathy," *Ophthalmology*, vol. 96, no. 1, pp. 80–86, 1989.

[32] A. F. M. Hani, T. A. Soomro, I. Fayee, N. Kamel, and N. Yahya, "Identification of noise in the fundus images," in *Proc. IEEE Int. Conf. Control Syst., Comput. Eng.*, 2013, pp. 191–196.

[33] K. Zuiderveld, "Contrast limited adaptive histogram equalization," *Graphics Gems IV*. San Diego, CA, USA: Academic, 1994, pp. 474–485.

[34] S. Irshad, X. Yin, L. Q. Li, and U. Salman, "Automatic optic disk segmentation in presence of disk blurring," in *Proc. Int. Symp. Vis. Comput.*, 2016, pp. 13–23.

[35] N. Otsu, "A threshold selection method from gray-level histograms," *IEEE Trans. Syst., Man, Cybern.*, vol. 9, no. 1, pp. 62–66, Jan. 1979.

[36] K. B. Khan, A. A. Khaliq, and M. Shahid, "B-COSFIRE filter and VLM based retinal blood vessels segmentation and denoising," in *Proc. Int. Conf. Comput., Electron. Elect. Eng.*, 2016, pp. 132–137.

[37] A. F. Frangi, W. J. Niessen, K. L. Vincken, and M. A. Viergever, "Multiscale vessel enhancement filtering," in *Proc. Int. Conf. Med. Image Comput. Comput.-Assisted Intervention*, 1998, pp. 130–137.

[38] S. Bouattour and D. Paulus, "Vessel enhancement in 2D angiographic images," in *Proc. Int. Conf. Functional Imag. Model. Heart*, 2007, pp. 41–49.

[39] C. K. Reddy and B. Vinzamuri, "A survey of partitional and hierarchical clustering algorithms," in *Proc. Data Clustering, Algorithms Appl.*, 2013, pp. 87–110.

[40] L. Kaufman and P. J. Rousseeuw, *Finding Groups in Data: An Introduction to Cluster Analysis*. Hoboken, NJ, USA: Wiley, 2009.

[41] P. J. Rousseeuw, "Silhouettes: A graphical aid to the interpretation and validation of cluster analysis," *J. Comput. Appl. Math.*, vol. 20, pp. 53–65, 1987.

[42] Y. B. Salem, K. Hamrouni, and B. Solaiman, "Image fusion models and techniques at pixel level," in *Proc. Int. Image Process., Appl. Syst.*, 2016, pp. 1–5.

[43] R. C. Gonzalez, R. E. Woods, and S. L. Eddins, *Digital Image Processing Using MATLAB*. Knoxville, TN, USA: Gatesmark Publishing, 2009.
[44] A. Hoover and M. Goldbaum, "Locating the optic nerve in a retinal image using the fuzzy convergence of the blood vessels," *IEEE Trans. Med. Imag.*, vol. 22, no. 8, pp. 951–958, Aug. 2003.
[45] T. Kauppi *et al.*, "DIARETDB0: Evaluation database and methodology for diabetic retinopathy algorithms," Mach. Vis. Pattern Recognit. Res. Group, Lappeenranta Univ. Technol., Finland, Tech. Rep., 2006.
[46] E. Decencière *et al.*, "Feedback on a publicly distributed image database: The messidor database," *Image Anal. Stereol.*, vol. 33, no. 3, pp. 231–234, 2014.
[47] A. Gastounioti, S. Makrodimitris, S. Golemati, N. P. E. Kadoglou, C. D. Liapis, and K. S. Nikita, "A novel computerized tool to stratify risk in carotid atherosclerosis using kinematic features of the arterial wall," *IEEE J. Biomed. Health Informat.*, vol. 19, no. 3, pp. 1137–1145, May 2015.
[48] R. F. Mansour, E. M. Abdelrahim, and A. S. Al-Johani, "Identification of diabetic retinal exudates in digital color images using support vector machine," *J. Intell. Learn. Syst. Appl.*, vol. 5, pp. 135–142, 2013.
[49] J. Odstrcilik *et al.*, "Retinal vessel segmentation by improved matched filtering: Evaluation on a new high-resolution fundus image database," *IET Image Process.*, vol. 7, no. 4, pp. 373–383, 2013.
[50] M. Ortega, M. G. Penedo, J. Rouco, N. Barreira, and M. J. Carreira, "Retinal verification using a feature points-based biometric pattern," *EURASIP J. Adv. Signal Process.*, vol. 2009, no. 1, pp. 235 746:1–235 746:13, 2009.
[51] Z. Waheed, M. U. Akram, A. Waheed, M. A. Khan, A. Shaukat, and M. Ishaq, "Person identification using vascular and non-vascular retinal features," *Comput. Elect. Eng.*, vol. 53, pp. 359–371, 2016.
[52] J. Staal, M. D. Abràmoff, M. Niemeijer, M. A. Viergever, and B. van Ginneken, "Ridge-based vessel segmentation in color images of the retina," *IEEE Trans. Med. Imag.*, vol. 23, no. 4, pp. 501–509, Apr. 2004.
[53] X. You, Q. Peng, Y. Yuan, Y. Ming Cheung, and J. Lei, "Segmentation of retinal blood vessels using the radial projection and semi-supervised approach," *Pattern Recognit.*, vol. 44, no. 10/11, pp. 2314–2324, Oct. 2011.
[54] J. V. B. Soares, J. J. G. Leandro, R. M. Cesar, Jr, H. F. Jelinek, and M. J. Cree, "Retinal vessel segmentation using the 2-D Gabor wavelet and supervised classification," *IEEE Trans. Med. Imag.*, vol. 25, no. 9, pp. 1214–1222, Sep. 2006.
[55] N. P. Singh and R. Srivastava, "Retinal blood vessels segmentation by using gumbel probability distribution function based matched filter," *Comput. Methods. Programs Biomed.*, vol. 129, pp. 40–50, 2016.
[56] E. Imani, M. Javidi, and H.-R. Pourreza, "Improvement of retinal blood vessel detection using morphological component analysis," *Comput. Methods Programs Biomed.*, vol. 118, no. 3, pp. 263–279, 2015.
[57] M. Vlachos and E. Dermatas, "Multi-scale retinal vessel segmentation using line tracking," *Comput. Med. Imag. Graph.*, vol. 34, no. 3, pp. 213–227, 2010.
[58] K. BahadarKhan, A. A. Khaliq, and M. Shahid, "A morphological hessian based approach for retinal blood vessels segmentation and denoising using region based Otsu thresholding," *PLOS ONE*, vol. 11, no. 7, pp. e0 158 996:1–e0 158 996:19, 2016.

Sidra Aleem received the B.Sc. degree in computer science from Fatima Jinnah Women University, Rawalpindi, Pakistan, in 2016. She is currently working toward the Graduate degree with the Department of Computer Science and Engineering, Shanghai Jiao Tong University, Shanghai, China.

Her research interests include image/video processing, biometrics analysis, computer vision, and machine learning.

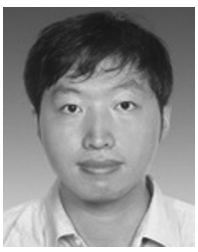

Bin Sheng received the Ph.D. degree in computer science and engineering from The Chinese University of Hong Kong, Hong Kong, in 2011.

He is currently an Associate Professor with the Department of Computer Science and Engineering, Shanghai Jiao Tong University, Shanghai, China. His current research interests include image-based rendering, machine learning, virtual reality, and computer graphics.

Ping Li received the Ph.D. degree in computer science and engineering from The Chinese University of Hong Kong, Hong Kong, in 2013.

He is currently an Assistant Professor with the Macau University of Science and Technology, Macau, China. His current research interests include image/video stylization, big data visualization, GPU acceleration, and creative media. He has one image/video processing national invention patent, and has excellent research project reported worldwide by *ACM TechNews*.

Po Yang received the B.Sc. degree in computer science from Wuhan University, Wuhan, China, in 2004, the M.Sc. degree in computer science from the University of Bristol, Bristol, U.K., in 2006, and the Ph.D. degree in electronic engineering from the Staffordshire University, Stoke-on-Trent, U.K, in 2010.

He is currently a Senior Lecturer with the Department of Computing Science, Liverpool John Moores University, Liverpool, U.K. He holds a strong tracking of high-quality publications and research experiences. He has published more than 40 papers. His current research interests include Internet of Things, RFID, and indoor localization, pervasive health, image processing, GPU, and parallel computing.

David Dagan Feng (F'03) received the M.Eng. degree in electrical engineering and computer science from Shanghai Jiao Tong University, Shanghai, China, in 1982, and the M.Sc. degree in biocybernetics and the Ph.D. degree in computer science from the University of California, Los Angeles, Los Angeles, CA, USA, in 1985 and 1988, respectively, where he received the Crump Prize for Excellence in medical engineering.

He is currently the Head with the School of Information Technologies, the Director in the Biomedical and Multimedia Information Technology Research Group, and the Research Director in the Institute of Biomedical Engineering and Technology, University of Sydney, Sydney, Australia. He has published more than 700 scholarly research papers, pioneered several new research directions, and made a number of landmark contributions in his field. More importantly, however, is that many of his research results have been translated into solutions to real-life problems and have made tremendous improvements to the quality of life for those concerned. He has organized/chaired more than 100 major international conferences/symposia/workshops, and has been invited to give more than 100 keynote presentations in 23 countries and regions.

Dr. Feng has served as the Chair in the International Federation of Automatic Control Technical Committee on Biological and Medical Systems. He is a fellow of the IEEE and Australian Academy of Technological Sciences and Engineering.